Analytical Methods

ROYAL SOCIETY OF CHEMISTRY

PAPER

View Article Online
View Journal

Cite this: DOI: 10.1039/d6ay00377j

Direct inlet probe mass spectrometry with wavelength selective resonance enhanced photo ionisation

Fabian Etscheidt,[abc] Philip Jürß,[ac] Christopher P. Rüger *[ac] and Ralf Zimmermann[acde]

We demonstrate a wavelength-selective atmospheric-pressure laser ionisation (APLI) workflow for direct inlet probe (DIP) evolved-gas analysis with ultra-high-resolution mass spectrometric detection. A tuneable optical parametric oscillator (213, 225, 248 and 266 nm) was integrated into a modified atmospheric-pressure ion source and coupled to Fourier-transform ion cyclotron resonance mass spectrometry (FT-ICR MS) to profile complex mixtures released directly from liquids and solids. Screening of over 70 aromatic standards revealed pronounced, compound-specific wavelength dependencies, with odd-electron molecular ions dominating and intensity maxima following known resonance-enhanced multiphoton ionisation (REMPI) band structures, enabling selectivity predictions based on the REMPI and APLI literature. Applied to fossil oils, oil blends, and asphaltenes, wavelength tuning systematically shifted molecular fingerprints while retaining aromatic selectivity in highly complex spectra (hundreds of assigned sum formulae per experiment). Shorter wavelengths (213/225 nm) emphasised naphthalene-type cores (double bond equivalent, DBE 7), whereas longer wavelengths (248/266 nm) enhanced phenanthrene/anthracene-type and more condensed aromatics (DBE 10–15). For polymers (polystyrene and crumb rubber), overall spectral patterns were less wavelength-dependent, but ion yields varied with wavelength, and additive signals (*e.g.*, *p*-phenylenediamine antiozonants) were readily detected alongside characteristic pyrolysis series. This DIP-APLI-FT-ICR MS approach enables rapid analysis of insoluble materials with minimal sample preparation while providing the ionisation wavelength as a practical "dial" to tailor selectivity and reduce spectral congestion at the ionisation stage. Thus, this technique broadens the capabilities of common DIP-MS approaches, which are dominated by chemical ionisation and lamp-based methods (APCI/APPI).

Received 3rd March 2026
Accepted 13th May 2026

DOI: 10.1039/d6ay00377j

rsc.li/methods

Introduction

Mass spectrometry has become an indispensable method in modern analytical chemistry. With the introduction of electrospray ionisation (ESI) in the 1990s,[1] the development of ionisation techniques has expanded rapidly over the last few decades, particularly taking advantage of the atmospheric pressure benefits allowing for robust operation, high flexibility and easy adaptations.[2] The choice of the ionisation technique strongly alters the detected molecular response; thus, selectivity and sensitivity of a workflow can efficiently be tailored to the research question and targeted analytes. Even within ESI, switching the polarity can markedly shift the observable chemical space, *e.g.*, by preferentially detecting acidic *versus* basic/neutral compounds.[3] However, deeper structural information by direct broadband mass spectrometry is often limited. To increase structural confidence, mass spectrometric strategies have therefore focused on tandem MS (precursor isolation and fragmentation) and chromatographic hyphenation.[4–6] More recently, the integration of ion mobility spectrometry, which adds an orthogonal descriptor related to ion size and shape *via* collision cross sections, has led to significant advances.[7,8] However, these attempts either focus on often complex separation or deal with the already generated ions. Thus, further exploration of the full capabilities of the actual ionisation process is favoured. In photoionisation, it has become evident that the choice of wavelength strongly alters the observed molecular response.[9,10] In particular, resonance phenomena, such as resonance-enhanced multi photon ionisation (REMPI) using UV photons to address aromatic compounds, show strong potential for wavelength-dependent analytical workflows.[11,12]

[a]*Joint Mass Spectrometry Centre/Chair of Analytical Chemistry, University of Rostock, 18059 Rostock, Germany. E-mail: christopher.rueger@uni-rostock.de*

[b]*Photonion GmbH, 19061 Schwerin, Germany*

[c]*Department Life, Light & Matter (LLM), University of Rostock, 18059 Rostock, Germany*

[d]*Department of Chemistry and Sustainable Technology, University of Eastern Finland, 80101 Joensuu, Finland*

[e]*Department of Environmental and Biological Sciences, 70211 Kuopio, Finland*

Recently, we introduced wavelength-resolved atmospheric pressure laser ionisation (APLI) deploying an OPO laser setup for scanning through 213–300 nm.[13] We could show that in direct infusion analysis, aromatic compounds exhibit characteristic spectroscopic fingerprints, which can be used for diagnostic procedures and structural elucidation. However, the standard approach in high-resolution mass spectrometry of "dilute and shoot", as used with electrospray, requires the samples to be soluble. Materials with limited solubility, such as polymers, heavy residues, or deposits, can be problematic or not accessible at all. Moreover, chemical interferences through charge transfer in the solvent evaporation process may occur. These limitations motivate the development of APLI workflows that retain wavelength-selective information while minimizing sample preparation and avoiding solubility constraints.

For insoluble materials and rapid screening tasks, evolved-gas analysis mass spectrometry has therefore become a common alternative.[14] In such approaches, controlled heating releases volatile and semi-volatile constituents from the bulk material, which are then transferred to ionisation and detection in mass spectrometric coupling. Numerous implementations exist, including direct inlet probe (DIP), atmospheric solids analysis probe (ASAP), and thermogravimetry-MS coupling (TGA-MS), with particularly widespread use in petroleomics and material science.[15–23] Among these, DIP is attractive because of its instrumental simplicity and speed, while still offering a degree of control through temperature settings or programmed ramps that can fractionate a sample by volatility and thermal stability. Depending on the temperature regime and heating profile, DIP can therefore provide rapid access to different chemical "windows" of a material (*e.g.*, additives and residual monomers at lower temperatures *versus* oligomeric fragments and thermal degradation products at higher temperatures), while requiring little to no sample preparation. Nonetheless, selectivity in many DIP-style workflows remains largely constrained by the available atmospheric-pressure ionisation (API) options and by the fact that ionisation is typically optimized for broad coverage rather than chemical-class specificity. This is particularly limiting for complex samples, where the number of detectable signals can quickly grow into the hundreds or thousands, and where targeted chemical questions benefit from reducing spectral congestion already at the ionisation stage. Encouraging work deploying soft atmospheric pressure photo and chemical ionisation (APPI/APCI) on natural[18] and anthropogenic polymers, polymer additives and heavy petroleum streams[16] have been presented. Hereby, mostly high-resolution mass spectrometry (HRMS) was used for detection. Given the often high complexity of the evaporated mixtures HRMS can be seen as pre-requirement for deciphering the different species and add chemical knowledge by accurate mass measurement and sum formula annotation. However, even though APPI and APCI gives access to different chemical space[18] and the addition of supporting agents adapts the ionisation process,[24,25] tailored analysis remains limited. Consequently, this research article is motivated by further expanding API capabilities in rapid thermal analysis, such as DIP-MS.

In this work, we report the first implementation of atmospheric-pressure laser ionisation (APLI) on a direct inlet probe (DIP) source combined with high-resolution mass spectrometric detection. By coupling DIP-based thermal desorption to a wavelength-selectable APLI scheme, we specifically target the wavelength-dependent selectivity. We hypothesize that changing the excitation wavelength will substantially modulate the molecular response of complex evolved-gas mixtures and thereby enable tuneable workflows. Guided by commonly used UV wavelengths for APLI/REMPI and practical laser availability, we investigated 213, 225, 248, and 266 nm, spanning a broad portion of the UV range relevant for REMPI-driven ionisation of aromatic constituents. To capture the chemical complexity released during DIP heating, often comprising isobaric and near-isobaric species across a wide m/z range, we employ Fourier-transform ion cyclotron resonance mass spectrometry (FT-ICR MS). Although FT-ICR MS provides lower spectral acquisition rates than scanning mass analysers, its ultra-high resolving power and mass accuracy enable confident sum-formula assignment and comprehensive molecular profiling of evolved-gas mixtures, including higher-m/z constituents that are particularly informative in petroleomics and polymer degradation studies. Wavelength effects are evaluated using (i) representative analytical standards, (ii) complex petroleum-derived mixtures, and (iii) anthropogenic polymer samples. The resulting datasets, typically containing hundreds of assigned sum formulas per experiment, are compared across wavelengths using compound-class grouping and molecular "fingerprint" visualizations such as DBE-based diagrams and related compositional maps. For petroleum samples and many common polymer thermal degradation products, pronounced homologous alkylation series are expected; therefore, we specifically assess how wavelength tuning shifts class distributions, homolog patterns, and DBE landscapes to reveal selectivity trends that can be exploited for improved interpretation of complex DIP-evolved mixtures.

Experimental

Material

For this study, four mixtures comprising in total more than 70 different aromatic compounds and PAHs were prepared in dichloromethane (DCM) at concentrations of 20–50 mg L^{-1} (Tables S1–S4). The complex samples were measured neat and consisted of four fossil oils, two asphaltenes and two polymeric materials: polystyrene (PS), and crumb rubber from used tyres (CR). The petroleum samples included a marine gas oil (MGO), a Colombian parent crude oil (PCO), a shale oil and an oil blend from the Caspian Pipeline Consortium (CPC). The asphaltenes were obtained from Athabasca bitumen by solvent deasphalting according to published procedures.[26,27] PS was purchased from Sigma-Aldrich ($M_w \sim 290\,000$, $M_n \sim 130\,000$; Merck KGaA, Darmstadt, Germany). The CR sample was taken from the Polymer Kit 1.0 of the Center for Marine Debris Research at Hawai'i Pacific University.[28]

Method

Ionisation setup. The ionisation source was a modified Bruker API source equipped with a direct inlet probe (DIP,

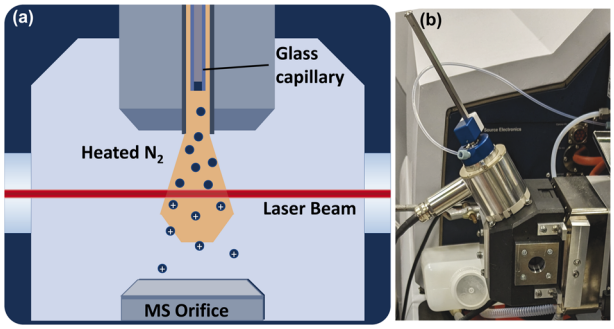

Fig. 1 (a) Scheme of the direct inlet probe atmospheric pressure laser ionisation setup featuring an optical parametric oscillator (OPO) and ultra-high resolution mass spectrometric detection (FT-ICR MS). (b) Photograph of the modified ion source. A photographic depiction is given in the SI (Fig. S01).

Bruker Direct Insertion Probe, Bruker Daltonics, Bremen, Germany). To enable laser ionisation, two fused-silica windows (UQG Optics Ltd, Milton, England) were installed on opposite sides of the source. The laser beam passed through the source perpendicular to both the vaporisation plume from the DIP/direct-infusion heater and the mass spectrometer inlet (Fig. 1). Prior to DIP laser-ionisation measurements, the laser beam path and source conditions were optimised using direct infusion of a diluted MGO solution.

As laser light source, an optical parametric oscillator (OPO; Opolette, Opotek, Carlsbad, CA, USA) with tuneable wavelength was used. Wavelengths of 213, 225, 248 and 266 nm were selected. The wavelengths 213 and 266 nm correspond to the fourth and fifth harmonics of a Nd:YAG laser, and 248 nm corresponds to the fundamental of a KrF excimer laser, all of which are commonly available commercially. The additional wavelength of 225 nm was chosen because previous studies reported particularly high sensitivity for higher-alkylated naphthalene-type species near this wavelength.[12,13] The laser operated at 20 Hz with a pulse width of 5 ns and a beam diameter of 4 mm. The laser pulse energy was monitored by a pyroelectric sensor and automatically adjusted to 120 μJ using a neutral-density filter wheel (Thorlabs GmbH, Bergkirchen, Germany). A more detailed description of the laser setup is given elsewhere.[13]

Sample introduction and vaporisation. Samples were introduced into the ion source in borosilicate melting-point determination capillaries (sealed at one end, DWK Kimble®, Merck KGaA, Darmstadt, Germany), which were plugged at the bottom with three fibreglass filter stamps (ADVANTEC, Grade QR-100, 0.38 mm thick), following a procedure established in the literature to prevent excessively rapid and non-reproducible DIP analysis.[18] Prior to use, capillaries and filters were baked for several hours out at 350 °C and 600 °C, respectively. Depending on sample volatility, the loaded samples were vaporised at 350 (for PCO) or 400 °C.

Mass spectrometric evolved gas analysis. High-resolution mass spectrometric measurements were performed in positive ion mode on a 7 T Bruker solariX Fourier transform ion cyclotron resonance (FT-ICR) mass spectrometer (Bruker Daltonics, Bremen, Germany). Spectra were acquired from m/z 100–1000 with a transient length of approximately 2 s (4 megawords, 4 M), providing a resolving power of ~320 000 at m/z 400 and a spectral acquisition frequency of approximately 0.5 Hz. The ion accumulation time was set to 300 ms, corresponding to an average of six laser shots. The source parameters were as follows: dry gas temperature, 180 °C; dry gas flow, 2.0 L min^{-1}; and nebuliser gas pressure, 2.5 bar. To focus on the lower and mid mass range (up to approximately m/z 1000), the time of flight was set to 0.7 ms.

Data processing and calibration. Pre-calibration of the acquired mass spectra was carried out in DataAnalysis 5.1 (Bruker Daltonics, Bremen, Germany) using a linear correction factor and sets of alkylated homologous series as internal calibrants. Peaks were picked with a signal-to-noise (S/N) threshold of 6, and the resulting time-resolved peak lists were exported using an in-house Visual Basic script. To account for mass shifts arising from space-charge effects associated with varying ion loads, the exported time-resolved data were automatically recalibrated on a spectrum-by-spectrum basis in CERES, a MATLAB-based (MathWorks, MATLAB R2024a) graphical user interface for calibration and annotation.[18,29] Molecular formula attribution was also carried out in CERES using an error window of ±1 ppm, yielding an average root-mean-square-error (RMSE) of 0.1545 ppm. The specific elemental constraints used for each sample type are summarised in Table S5 (SI).

Results and discussion

Direct inlet probe mass spectrometry has been established as a robust and versatile approach for the analysis of viscous and solid samples, often poorly soluble or insoluble materials. In this work, the evaporated and laser-ionised compounds are monitored by ultra-high-resolution FT-ICR MS operated at a relatively low acquisition frequency of ~0.5 Hz, thereby placing emphasis on resolving power and mass accuracy rather than temporal resolution. The analytical standards evaporate rapidly, allowing the acquisition and averaging of approximately 15–30 scans (approx. 0.5–1 min total acquisition time), whereas the complex mixtures, particularly the polymer samples, exhibit significantly longer evaporation times of up to 10 min. As the main objective of this study is to compare the ionisation characteristics of different APLI wavelengths, a constant vaporisation temperature is employed for each sample type. Consequently, thermal release profiles and related phenomena, which have been discussed extensively elsewhere,[16,30,31] will not be treated in detail in the following.

Analytical standard compounds

Out of the 73 standard compounds investigated, 45 were detected at least at one wavelength (Tables S1–S4). Most of these (~75%) were ionised at all four wavelengths, albeit with markedly different signal intensities. In contrast, several low-mass ($<m/z$ 150) aromatics, quinone-type species, nitro-PAHs and specific nitrogen-containing PAHs were not observed under the

present conditions. Overall, DIP-APLI predominantly yields aromatic radical cations with only limited protonation, in line with previous observations for REMPI/APLI and APPI sources.[32,33]

Low-mass compounds below m/z 150, such as indole or benzofuran, were not detected, although they have previously been observed by REMPI MS.[34] This is most likely due to the discrimination of low m/z ions that is typical for FT-ICR MS, placing these species at the lower edge of the practically accessible mass range.[35] This interpretation is supported by the clear detection of the methylated indole derivative, which is both heavier and expected to exhibit a higher ionisation cross section due to alkylation.[12] A similar limitation applies to substituted benzene derivatives which, depending on their substitution degree, also populate the lower m/z range and are further disfavoured by the generally lower ionisation cross sections of single-ring aromatics compared with fused PAHs.[12,36] The remaining homo-atomic PAHs were all observed as odd-electron molecular radical cations ($[M]^{\bullet+}$), except for acenaphthylene. The latter is known to be difficult to ionise by (multi-photon) photoionisation due to the short lifetimes of its excited states, which hamper the absorption of a second photon to reach the ionisation continuum.[10,37]

For the heteroatom-containing PAHs, most sulphur- and oxygen-containing compounds with ring-bound heteroatoms and at least three conjugated rings were readily detected, consistent with the higher ionisation cross sections of larger, more extensively conjugated systems.[12] A notable exception is dibenzothiophene-*S*,*S*-dioxide, which was not observed. This is most plausibly attributed to the absence of free electron pairs at the sulphur bridge and, thus, a reduction of electron delocalisation over the aromatic framework, reducing the ionisation efficiency. Quinone-type PAHs were likewise not detected, even though their UV spectra show absorption bands in the relevant wavelength range.[38] Electron-withdrawing (–I, –M) carbonyl groups destabilise the intermediate excited state and increase the ionisation potential, which likely results in low ionisation cross sections.[39] In line with this reasoning, fluorenone is not visible in the mass spectra, whereas anthrone, in which the carbonyl functionality is less conjugated, is only weakly ionised.

Nitrogen-containing PAHs show a pronounced dependence on the type of ring-bound nitrogen. PAHs with pyrrolic (five-membered) nitrogen, such as carbazole, as well as alkylated indole, are efficiently ionised as long as they comprise at least three rings or carry an alkyl substituent. In contrast, acridine, where the nitrogen is part of a six-membered (pyridinic) ring, does not yield a detectable radical cation. This behaviour has previously been reported for acridine and other six-membered nitrogen heterocycles such as pyridine and is commonly attributed to the short excited-state lifetimes of pyridinic species, which interferes efficient multiphoton ionisation.[12,32,40,41] However, while the radical cation is not observed for acridine, the protonated molecule $[M + H]^+$ is detected at all wavelengths. The protonation behaviour of the nitrogen PAHs reflects their basicity and electronic structure. Pyrrolic species show no protonation, as the nitrogen lone pair is part of the aromatic πsystem, which lowers their basicity considerably. This is consistent with previous observations in APPI.[42] In contrast, acridine and related imine-like compounds possess a more available lone pair and therefore higher basicity, favouring $[M + H]^+$ formation. The compound 1,1,2-trimethylbenz[*e*]indole illustrates this behaviour particularly well: its imine-like nitrogen leads to a basicity comparable to acridine, and both the radical cation and protonated even-electron species are observed.

Among PAHs bearing nitrogen-containing functional groups, only naphthylamine was detected. None of the three nitro-PAHs were observed, although the corresponding parent PAHs are readily ionised at all wavelengths used, which would in principle support ionisability of the substituted derivatives. The difference between amine and nitro functionalities can again be rationalised in terms of their electronic effects: the amine group is electron-donating and stabilises both the intermediate excited state and the ionised state, whereas nitro groups are strongly electron-withdrawing and significantly increase the ionisation potential, as known for nitrobenzenes.[39] This is analogous to the effect of carbonyl groups in the quinone-type PAHs discussed above. Moreover, several nitro-aromatic explosives, such as 2,4,6-trinitrotoluene, have been reported to undergo photodissociation of the nitro group upon UV irradiation, yielding nitrogen oxide fragments.[43–45] It appears likely that similar photodissociation processes occur for the nitro-PAHs studied here, further suppressing the formation of intact molecular radical cations. Such fragmentation can be suppressed by using a short-pulse femtosecond laser for ionisation, whereby the compounds are ionised *via* a second photon before dissociation occurs. Compounds with short excited-state lifetimes, such as acenaphthylene, may likewise be ionised in this way when the pulse duration matches the excited-state lifetime.[46–48]

When comparing different wavelengths, pronounced differences emerge in the mass spectra of the standard mixtures. For solution M4, the most prominent peak shifts from coronene (m/z 300) at 213 nm to 2-methylanthracene (m/z 192) at 225/248 nm and retene (m/z 234) at 266 nm, indicating a wavelength-dependent selectivity for specific compounds in DIP-REMPI (Fig. 2). This is especially evident for naphthalene and its alkylated derivatives. Naphthalene itself is only detectable at 213 and 266 nm, while 2-methylnaphthalene is observed at 213, 225 and 266 nm. 2-Ethylnaphthalene is detectable at all wavelengths, but its signal intensity varies strongly; the weakest signal is only ∼2% of the strongest one at 248 and 213 nm, respectively (Fig. 2). These trends agree well with literature REMPI spectra, which exhibit the dominant band between 213 and 300 nm centred around 216 nm and a considerably weaker band near 270 nm.[12,13] For all alkylated naphthalenes, including acenaphthene, the intensity at 266 nm is consistently higher than at 248 nm but lower than at 213 and/or 225 nm, in line with the most intense REMPI features occurring at the shorter wavelengths.[12,13]

The reported redshift of REMPI bands with increasing degree of alkylation is also reflected in the wavelength-dependent intensities. The ratio of signal intensities at 213 and 225 nm decreases from a factor of 4.5 for 2-

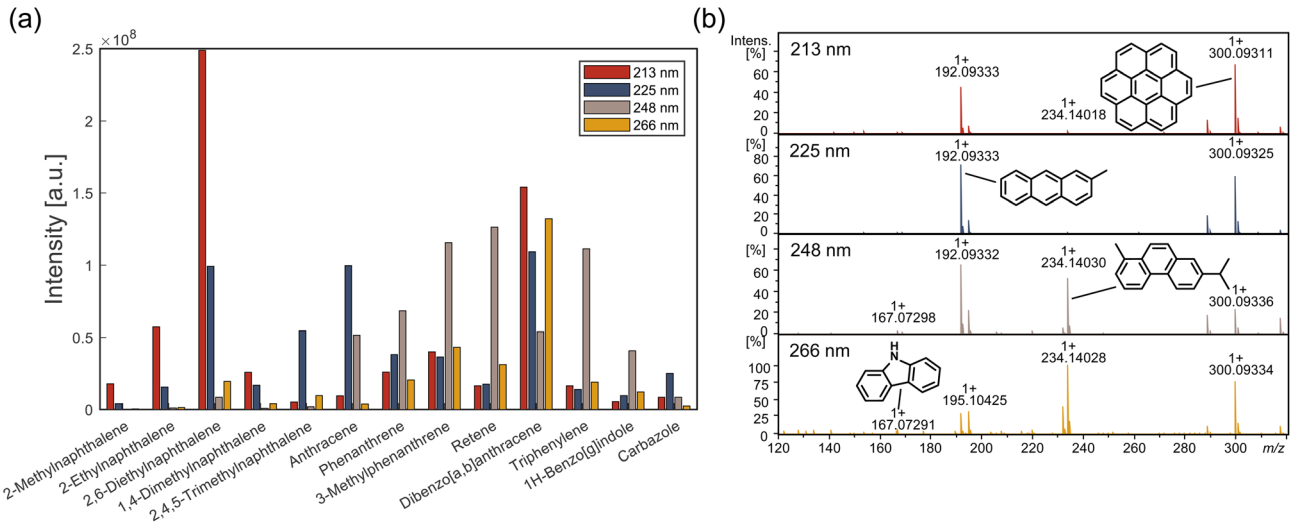

Fig. 2 (a) Summed intensities for selected standard species at the four investigated wavelengths. (b) Mass spectra of the standard solution M4 at, from top to bottom, 213 nm, 225 nm, 248 nm, and 266 nm.

methylnaphthalene to 1.5 for 1,4-dimethylnaphthalene, and for 2,4,5-trimethylnaphthalene the maximum intensity is observed at 225 nm. Three-ring aromatics based on anthracene and phenanthrene, by contrast, show their highest intensities in spectra recorded at 225 and 248 nm, respectively, consistent with the redshift of the main REMPI band caused by the larger conjugated system.[49,50] Although the intensity differences for phenanthrene are less pronounced than for the naphthalene-type species (a factor of ~3 between 248 and 266 nm), the intensity spread increases considerably for more strongly alkylated derivatives, reaching a factor of almost one order of magnitude between 248 and 213 nm for retene. Differences in band position and shape between anthracene and phenanthrene are also reflected in their intensity patterns: anthracene shows the highest signal at 225 nm, in accordance with its narrower, more blue-shifted REMPI band compared with phenanthrene. Other isomeric structures, such as 1*H*-benzo[*g*]indole and carbazole, also display different optimal wavelengths (maxima at 248 and 225 nm, respectively), again matching expectations based on their literature spectra.[13] Triphenylene exhibits a particularly strong wavelength selectivity, with the intensity at 248 nm being 5.8 times higher than at 266 nm, which is consistent with its sharp REMPI band centred at 249 nm.[12]

In contrast to conventional APPI or APCI, which can be susceptible to the formation of oxidation artefacts,[51] no appreciable levels of oxidised products were detected at any wavelength in the present DIP-APLI experiments, despite fresh ambient air being introduced into the ion source with each sample injection. Overall, DIP-APLI behaves in line with other REMPI-type ion sources: spectra are dominated by aromatic radical cations, protonation is largely confined to more basic nitrogen-containing species, and tuning the excitation wavelength imposes pronounced molecular selectivity that closely follows the REMPI band structures of the investigated PAHs. By comparison, APPI, commonly employing a krypton discharge lamp (10.0/10.6 eV), is operationally closer to single-photon ionisation (SPI). With alternative VUV sources (*e.g.*, excimer lasers at 157 nm (7.9 eV)[9] or xenon lamp fillings at 9.6/8.4 eV (ref. 10)), even SPI could, in principle, introduce an additional selectivity dimension without full wavelength scanning at a synchrotron, but was not explored here. A useful perspective emerges when comparing atmospheric-pressure DIP-HRMS with established vacuum DIP-HRMS implementations (*e.g.*, vacuum DIP-HRT using HR-ToF). In vacuum, DIP-based evaporation is often more straightforward to realise and control, but the standard ionisation option on HR-ToF platforms remains electron ionisation (EI),[22,23] and implementing photoionisation in vacuum DIP is technically demanding. In contrast, although DIP at atmospheric pressure is inherently more challenging from an EGA standpoint, it offers more accessible coupling to soft photoionisation concepts within standard atmospheric-pressure ion sources and high-resolution analysers, such as FT-ICR MS. Beneficially for these atmospheric-pressure photoionisation regimes, matrix effects are reported to be markedly lower than for APCI, while different chemical subspaces can be preferentially addressed, effectively changing the "chemical glasses" through which complex mixtures are viewed.

Complex samples

While the standard mixtures demonstrate that the DIP-APLI source behaves as expected and that the excitation wavelength can be used to tune the response of defined PAH structures, the main strength of DIP lies in the analysis of complex mixtures with minimal sample preparation. In contrast to the standards, which contain fewer than 20 compounds, spectra of complex samples easily comprise more than a thousand peaks per measurement.[16,18] These peaks include both target analytes and matrix components that may not be relevant to a given analytical question. It is therefore advantageous if the ionisation technique itself can provide a degree of selectivity towards

specific analyte classes, thereby reducing the effective spectral complexity. REMPI has long been used in this way to selectively ionise PAHs in complex matrices, particularly in environmental analysis where PAHs are of interest due to their carcinogenic and toxic properties. As shown above for the standards, tuning the excitation wavelength in DIP-APLI further allows a selective enhancement of particular PAH subclasses and core structures. At the same time, the high molecular diversity in fossil-based oils and bitumen increases the likelihood of ion–molecule reactions and ion suppression effects that may compromise this selectivity. Owing to their richness in aromatic species, fossil oils, oil blends and asphaltenes are, nevertheless, ideally suited to be probed by APLI-based methods.[10,52–54]

Petroleomics

Consistent with the standard compounds, DIP-APLI of the complex petroleum samples predominantly yielded odd-electron radical species, especially among CH-class species. An exception was an alkylated series with a double bond equivalent of 11.5 observed in some of the higher-boiling samples (Fig. S07). This series has previously been described in the literature and assigned to the photofragmentation of highly alkylated phenanthrenes.[55] However, its contribution remained substantially lower than that of the corresponding unfragmented phenanthrene radical-ion series. The REMPI-DIP measurements of a marine gas oil (MGO) at 266 nm exhibit the typical evaporation profile of fully or predominantly vaporisable oils.[16] The total ion current rises sharply within a few seconds, reaches a maximum, and then decays rapidly so that most of the signal intensity is lost within approximately two minutes, followed by a slowly decreasing tail (Fig. 3a). A similar trend was observed for the oil blend, whereas the asphaltenes exhibited a slower signal decay, likely due to the presence of higher-boiling or pyrolysing constituents. The compound-class distribution is not uniform across this desorption peak. At the apex, the relative contributions of CHN and CHO species increase to 28% and 21%, respectively, at the expense of the CH class, while their averages over the entire desorption profile are only 5.3% and 5.1%. Together with low odd/even ratios for the CHN class (3.4) this suggests enhanced ion–molecule chemistry and/or ion suppression during the phase of highest analyte concentration, consistent with the general concentration dependence of such effects.[56] Despite this additional complexity, replicate measurements are highly reproducible. Triplicate spectra acquired at each wavelength yield congruence coefficients > 0.99 (Fig. 3), demonstrating that the DIP-APLI response is stable even for complex matrices. In contrast, congruence coefficients between spectra recorded at different wavelengths can be as low as 0.3, indicating that the wavelength-dependent selectivity observed for the standard compounds is preserved in the complex mixture. The most similar pairs are again the adjacent wavelengths: spectra at 213 and 225 nm, and at 248 and 266 nm, show higher mutual congruence (typically >0.96 and >0.92, respectively) than with the more distant wavelengths (Fig. 3c). Part of these differences arises from variations in the number of shared and unique elemental compositions. For MGO, ionisation at 266 nm yields 552 assigned sum formulas, of which 509 are shared with at least one of the other wavelengths (Fig. 3b). In contrast, measurements at 213 and 225 nm produce 92 and 270 additional unique attributions, respectively, and a further 232 sum formulas are shared exclusively between these two wavelengths. A similar trend is observed for the other fossil samples (Fig. S02), where the highest numbers of unique assignments are typically found at 213 or 225 nm. In addition to these presence/absence effects, substantial differences in relative intensity are observed for compositions that are common to all wavelengths.

These intensity patterns are accessibly visualised in double bond equivalent (DBE) *versus* carbon number plots (Fig. 4), where the DBE provides an upper estimate of the size of the fused aromatic core, which strongly influences ionizability in REMPI MS. For the CH class, the most pronounced differences occur between the lower (213, 225 nm) and higher (248, 266 nm) wavelengths. At 213 and 225 nm, species with DBE 7 and 8 are

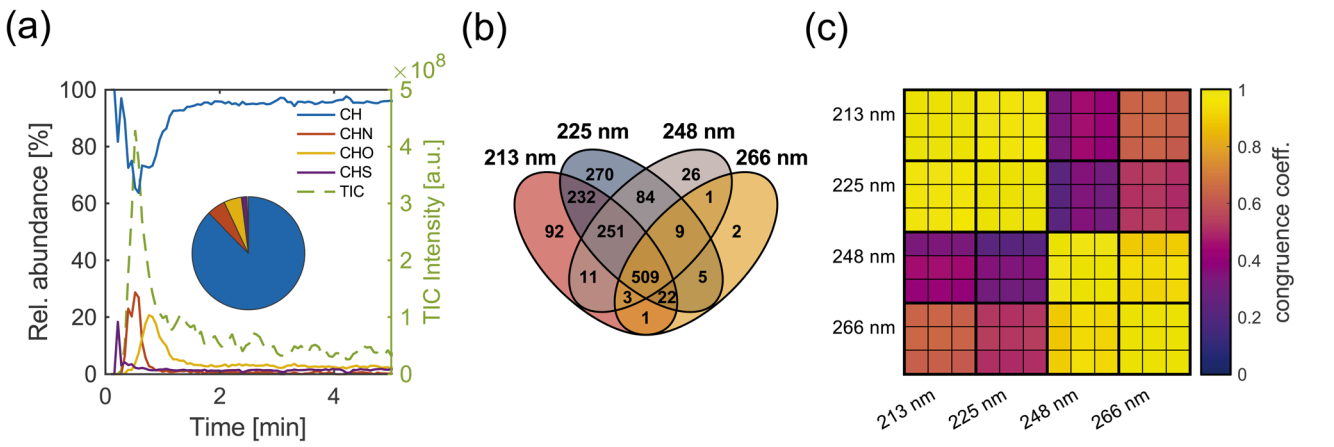

Fig. 3 (a) Total ion chromatogram of MGO measured at 266 nm, with relative abundance of each compound class. The relative abundance over the whole measurement are given in the pie chart. (b) Venn diagram of assigned compounds for MGO at different wavelengths. (c) Heatmap of congruence coefficients between spectra measured at different wavelengths. For each wavelength, three DIP experiments were acquired, and a separate congruence coefficient was calculated.

particularly prominent, whereas they contribute only weakly at 248 and 266 nm. Conversely, compositions with DBE 10 show elevated relative intensities at 248 and 266 nm. This pattern is observed consistently for all six investigated fossil samples and mirrors both the behaviour of the standard compounds and the general PAH composition of fossil oils, where DBE 7 and 10 species are commonly associated with naphthalene and phenanthrene/anthracene cores, respectively.[57] As shown above for the standards, naphthalene-type cores exhibit strong REMPI bands at shorter wavelengths with only weak absorption towards the red, whereas phenanthrene-type species have intense bands around 248 nm.[12,13] The wavelength-dependent enrichment of DBE 7 at 213/225 nm and DBE 10 at 248/266 nm in the complex samples is therefore an indicator of the same spectral features. For samples with higher contents of larger aromatics, such as the crude oil and asphaltenes, even

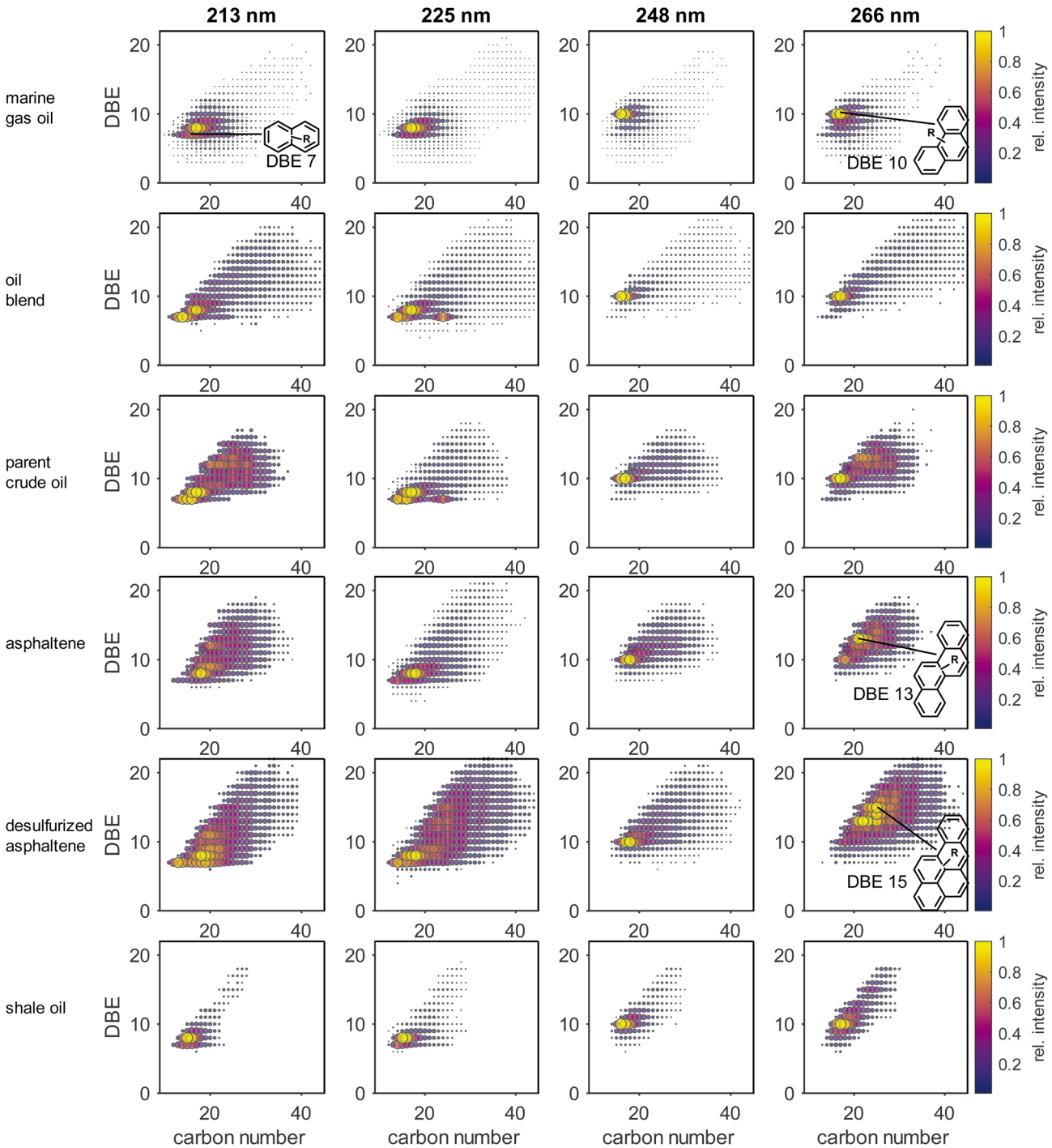

Fig. 4 DBE *versus* carbon number plots for the CH-class of the fossil oil samples measured at, going from left to right, 213 nm, 225 nm, 248 nm, and 266 nm, with the relative intensities of each species in a measurement and selected tentatively assigned structures.

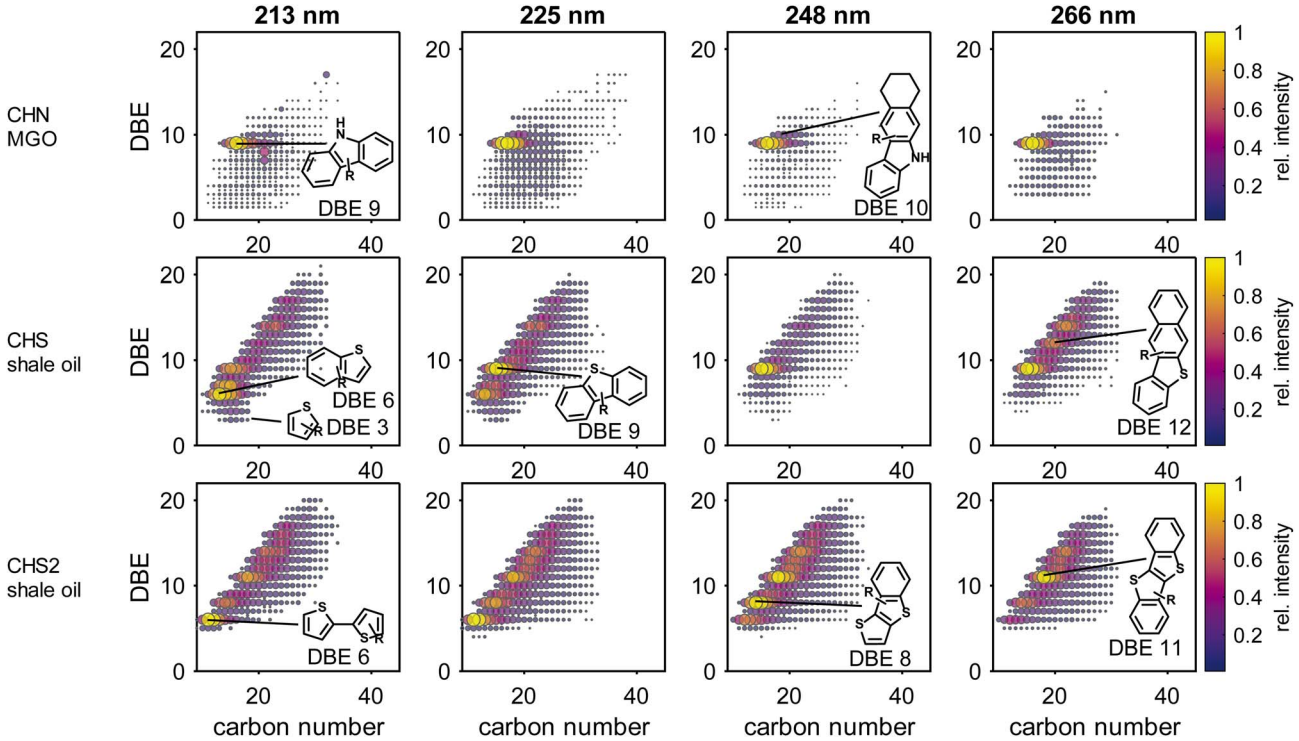

Fig. 5 DBE *vs.* carbon number plots for the CHN-class of MGO and the CHS- and CHS_2-class of the shale oil as examples for heteroatom classes of the fossil oil samples measured at, going from left to right, 213 nm, 225 nm, 248 nm, and 266 nm, with the relative intensities of each species in a measurement and selected tentatively assigned structures.

higher DBE species become relatively more abundant at 266 nm than at the lower wavelengths. In particular, DBE 13 compositions show markedly increased intensities at 266 nm. These are most likely associated with four-ring cata-condensed aromatic cores, whose excited states are further red-shifted compared to their two- and three-ring analogues owing to the larger delocalised π-electron system.[49,58,59] Similarly, DBE 15 species, which likely correspond to peri-condensed PAHs such as benzo[*a*]pyrene that have strong REMPI responses around 266 nm, are enhanced in the asphaltene spectra recorded at this wavelength. Overall, for the fossil oils, increasing the excitation wavelength shifts the CH-class distribution towards higher DBE values as the REMPI bands of larger aromatic structures are progressively accessed, whereas the lower wavelengths reveal smaller naphthalene-type aromatics that remain largely undetectable at 248 and 266 nm.

For heteroatom-containing PAHs, the wavelength effects are generally less pronounced than for the CH class but still show characteristic trends. The CHN class exhibits a higher degree of protonation *via* ion–molecule reactions than the other classes, reflecting the basicity of some nitrogen functionalities, although odd-electron radical cations remain the dominant ion type overall (Fig. 5 and 6). Protonated species typically form smooth, continuous DBE distributions, reflecting the Boduszynski continuum,[60] and on average occur at lower DBE than the directly photoionised radical ions, which tend to appear only above a certain DBE threshold and often show pronounced maxima at specific DBE values. Interestingly, DBE 10 CHN compositions, which would correspond to alkylated acridine-type structures if they were pyridinic, do not exhibit elevated protonation levels in the fossil oils, even when they constitute the second most abundant DBE class, as in MGO. This contrasts sharply with the behaviour of acridine in the standard mixture, where only $[M + H]^+$ ions were observed at all wavelengths with no detectable radical cations. The complex-sample data therefore suggest that the DBE 10 CHN species predominantly comprise neutral (non-pyridinic) nitrogen compounds, which are known to be more abundant than pyridinic species in fossil oils.[61,62] Structures such as carbazole derivatives fused with an additional saturated six-membered ring are plausible candidates.[63] The extent of protonation within the CHN class is also sample dependent; the oil blend and asphaltene, for example, show a substantially lower fraction of odd-electron ions than the other oils (Fig. S03 and S08).

Across all oil samples and wavelengths, there is a pronounced increase in CHN intensity at DBE 9, consistent with readily ionisable *N*-PAHs such as carbazoles and benzoindoles (Fig. 6 and S08). For most samples, DBE 12 species (benzocarbazoles) stand out from the distribution and represent the most abundant CHN subclass. Exceptions are MGO, which – given their lower distillation cut – contains fewer highly condensed *N*-PAHs, and the shale oil, where DBE 11 species dominate over DBE 12 at all wavelengths except 266 nm. The CHS and CHS_2 classes are again clearly wavelength dependent, particularly in the sulphur-rich shale oil, and show only minor protonation, with intensity-weighted odd/even ratios above 200

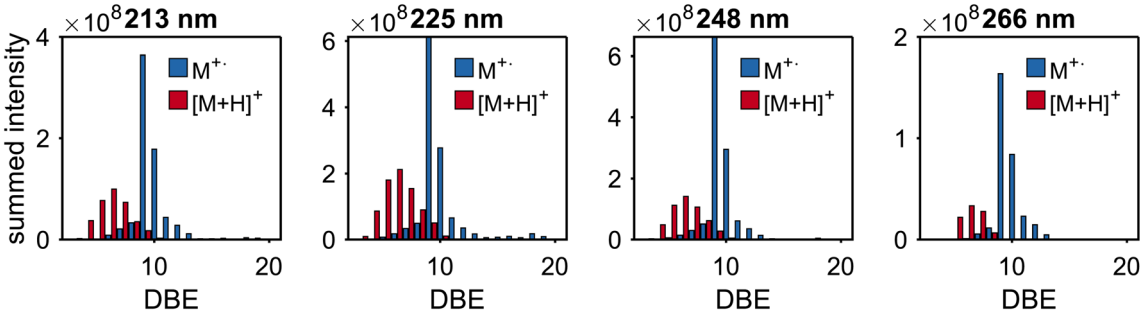

Fig. 6 DBE distribution of the CHN class of MGO measured at, going from left to right, 213 nm, 225 nm, 248 nm, and 266 nm. The red bars represent even electron species, while the blue ones represent odd electron species as visual guidance.

and 90, respectively. At 213 nm, the lowest observed DBE in the CHS class is 3, and the most prominent species have DBE 6, consistent with thiophenes and benzothiophenes.[64] As the excitation wavelength increases, the dominant CHS species shift to DBE 9, while thiophenes become undetectable. The CHS_2 class follows the same trend: at short wavelengths, DBE 6 compositions (bithiophenes)[64] dominate, at intermediate wavelengths DBE 8 species (benzodithiophenes)[65] are most intense, and at 266 nm DBE 11 species prevail, in agreement with the strong REMPI bands reported for naphthodithiophenes at this wavelength.[13] This progression closely mirrors the behaviour observed for the CH class and can likewise be rationalised by the decreasing energy of the lowest excited states with increasing DBE. Larger π-systems with higher DBE can be efficiently ionised at longer wavelengths, whereas smaller systems, such as thiophenes, require shorter wavelengths for effective REMPI ionisation.

Taken together, these results show that, even in highly complex fossil-derived matrices where ion–molecule reactions and suppression effects are possible, DIP-APLI retains a robust, wavelength-dependent molecular selectivity that is fully consistent with the REMPI behaviour established for the PAH standards.

Polymers

In addition to liquid and semi-liquid fossil-derived samples, DIP-APLI also enables the direct analysis of solid materials. To explore this capability, two representative polymeric samples, polystyrene and crumb rubber, were investigated. In contrast to the fossil oils discussed above, which exhibit a typical desorption-dominated profile (often accompanied by partial thermal decomposition depending on volatility), the DIP signals of both polymers are largely governed by pyrolysis processes due to the macromolecular nature of the polymer chains. As a result, the total ion current shows a slower rise in intensity and broader DIP peaks, which can extend over more than 10 min (Fig. 6). An exception is formed by low-molecular-weight additives, whose ion traces display a sharp rise in intensity followed by a rapid decay, characteristic of desorption-controlled behaviour.

In comparison to the fossil oils, the polymers exhibit comparatively small mass spectrometric differences between the four excitation wavelengths. Congruence coefficients remain above 0.83 for crumb rubber and 0.93 for polystyrene (Fig. S12), indicating that the overall spectral patterns are much less wavelength dependent than for the petroleum samples. This can largely be ascribed to the more homogeneous chemical composition of the polymers with respect to REMPI-active chromophores. In the case of polystyrene, the relevant chromophore is essentially limited to the phenyl moiety of the styrene repeat unit. Nevertheless, clear differences in overall signal intensity are observed between the four wavelengths. Polystyrene shows the highest total signal at 248 and 266 nm, in agreement with the $S_1 \leftarrow S_0$ transition of alkylbenzenes, which lies in this spectral region,[66] whereas crumb rubber is most efficiently ionised at 225 nm (Fig. S13). The mass spectra of polystyrene exhibit peak clusters separated by 104 u, corresponding to di-, tri- and tetramers of styrene (C_8H_8 monomer) formed by thermal degradation. This behaviour is even more clearly visible in DBE *versus* carbon number plots (Fig. 6), where distinct signal groupings are separated by eight carbon atoms and four DBE, matching the styrene monomer unit. These observations are consistent with previous reports on polystyrene pyrolysis behaviour.[67]

Crumb rubber differs from polystyrene in that it does not only show a broad pyrolysis profile but also a pronounced initial evaporation phase dominated by CHN_2-class species. This phase gives rise to a comparatively sharp TIC peak at the beginning of the experiment. The main constituent of this evaporation peak has the sum formula $C_{18}H_{24}N_2$ and most likely corresponds to *N*-(1,3-dimethylbutyl)-*N*′-phenyl-*p*-phenylenediamine (6PPD), a widely used antiozonant in rubber products.[68,69] The remaining CHN_2 species are plausibly related phenylene diamine antiozonants and/or their degradation products. After this initial desorption of additives, a slower, long-lasting pyrolysis phase of the rubber polymer chains follows, analogous to the behaviour observed for polystyrene (Fig. 6). This pyrolysis phase is dominated by CH and CHS classes. Although the CH class displays a broad, nearly continuous distribution with DBE values ranging from 4 to 19 and carbon numbers from 10 to 50, the DBE *versus* carbon number plot still reveals a repeating pattern of five carbon atoms and one DBE. This pattern matches the repeat unit of polyisoprene (C_5H_8), the main constituent of natural rubber, which has

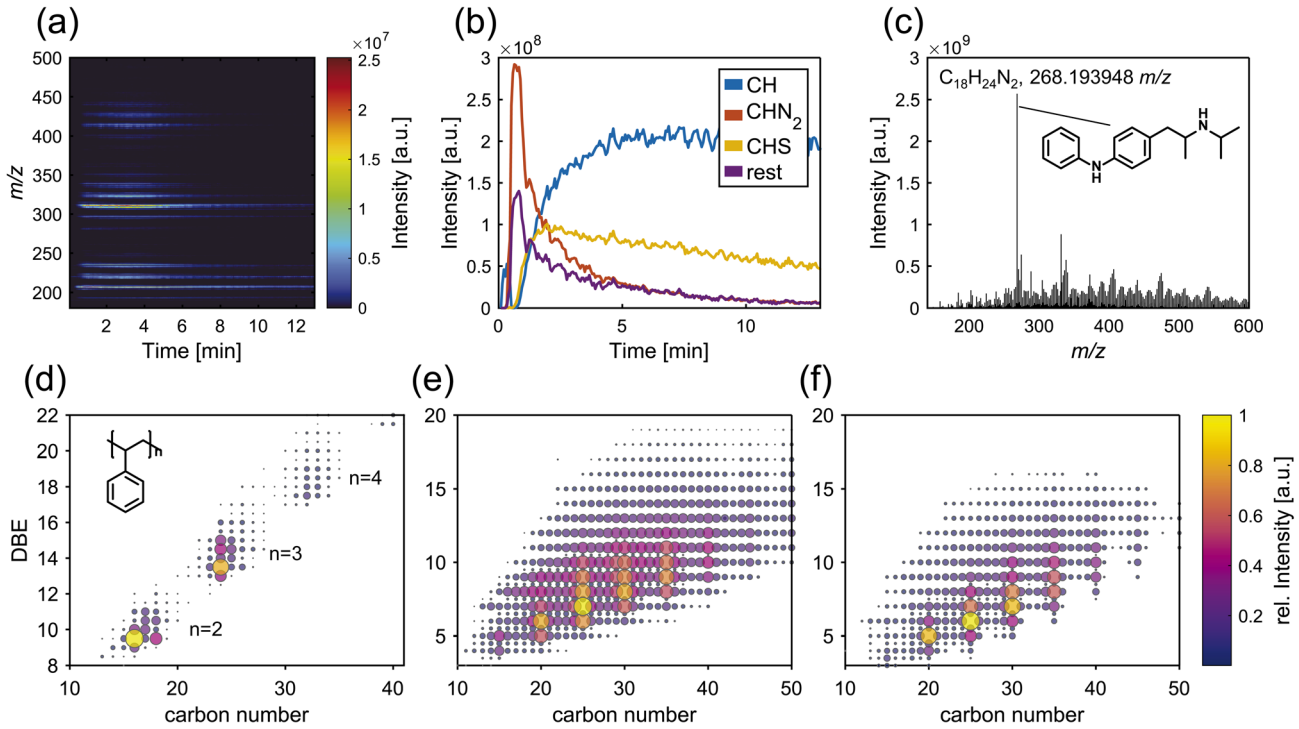

Fig. 7 (a) Survey view of the DIP measurement of PS visualising time-trend *versus* molecular profile (*m*/*z*), (b) temporal release profile for selected compound classes of rubber, (c) summed line mass spectra for the crumbed rubber sample. Carbon number *versus* DBE plots for the DIP measurement of: (d) the CH-class of PS, (e) the CH-class of crumbed rubber, and (f) the CHS-class of crumbed rubber.

a degradation temperature below 400 °C, in contrast to some synthetic rubbers.[70] The CHS class essentially mirrors the CH class, reflecting the same polymeric backbone with the addition of sulphur introduced during vulcanisation.

Taken together, the polymer results complement the findings from the standards and fossil oils: (I) DIP-APLI can effectively probe both additive desorption and backbone pyrolysis in solid polymer samples; (II) the wavelength dependence is muted when the underlying chromophore variety is low (polystyrene), but still manifests in overall ionisation efficiency; and (III) DBE *versus* carbon number maps remain a powerful tool to recognise repeating units and structural motifs, even in thermally fragmented polymer-derived mixtures (Fig. 7).

Conclusion

In this study, we extend the established APLI concept for direct inlet probe (DIP) measurements by implementing a wavelength-tuneable laser source. In contrast to ionisation schemes commonly used in DIP, such as APPI, which offers broad ionisability, and APCI, which favours slightly polar components, APLI provides a distinct selectivity towards aromatic compounds and thus complements existing DIP ionisation approaches. Screening more than 70 aromatic standards at four excitation wavelengths (three of which correspond to widely available laser lines) revealed pronounced, analyte-specific wavelength effects and selectivity differences. Crucially, the observed response patterns followed known REMPI band structures reported for other introduction techniques, demonstrating that wavelength-selective REMPI behaviour transfers well to the DIP workflow and enabling the use of existing REMPI literature to anticipate compound-specific responses.

In addition to the standard solutions, several fossil oils and polymer samples were measured as representative complex mixtures. The fossil oils showed the typical highly aromatic CH-class distribution commonly observed for APLI direct infusion spectra of these sample types. In contrast to direct infusion, however, these spectra were obtained directly from neat samples without any sample preparation such as filtration, extraction, or dilution. Moreover, the measurements were comparatively fast, as the DIP process was dominated by rapid evaporation. Although there are indications of slightly elevated levels of ion chemistry (*e.g.*, charge transfer reactions), particularly affecting CHN-class species, the overall selectivity towards aromatic compounds, especially within the CH class, was preserved, as no species with DBE values below that of a single benzene ring were detected. Wavelength-dependent differences remained clearly observable: the shorter wavelengths (213 and 225 nm) favoured naphthalene-type species (DBE 7), whereas the longer wavelengths (248 and 266 nm) enhanced phenanthrene-/anthracene-type species (DBE 10) and even larger condensed aromatic structures. In the heavier oils, compositions with DBE 13 and 15, corresponding to up to five fused rings, were particularly enhanced at the higher wavelengths.

The polymer samples exhibited smaller spectral differences between wavelengths than the fossil oils, which can be attributed to the more homogeneous composition of polymers with respect to REMPI-active chromophores, such that ionisation is largely governed by the same functional motif within a given polymer. Here, the dominant wavelength effect was therefore mainly reflected in differences in overall ionisation yield. Beyond the expected pyrolysis fragments, which matched literature descriptions, typical additives were also detected, such as 6PPD in rubber. While these additives appeared among the dominant signals in an untargeted workflow, the demonstrated wavelength selectivity suggests that the excitation wavelength could be tuned towards the ionisation maximum of specific target compounds to enable targeted trace analysis. This aspect is beyond the scope of the present work, but will be investigated in future studies. In addition, the implementation of temperature ramping is expected to reduce the simultaneous ion load and further improve selectivity and sensitivity by mitigating ion suppression, while also prolonging signal duration and thereby enhancing spectral quality.

Author contributions

F. E. conceptualisation, data curation, formal analysis, methodology, software, validation, visualization, writing – original draft; P. J. data curation, formal analysis, investigation, methodology, validation, writing – review & editing; R. Z. funding acquisition, project administration, resources, supervision, writing – review & editing; C. P. R. conceptualisation, methodology, project administration, software, supervision, writing – original draft.

Conflicts of interest

The authors declare that they have no known competing financial interests or personal relationships that could have influenced the work reported in this paper. However, Fabian Etscheidt is linked to the University of Rostock spin-off, Photonion GmbH, which manufactures and distributes custom photoionisation mass spectrometers. All images in the main body figures, the TOC figure, and the SI were created by one of the authors.

Data availability

Data for this article, including the time-resolved sum formula annotation of the DIP experiments as well as time-averaged data with mass error and abundance values, are available at The Open Science Framework (OSF, https://osf.io) at https://doi.org/10.17605/OSF.IO/HS4DA.

Supplementary information (SI): composition and detection of the standard mixtures (Tables S1–S4); parameters for sum formula annotation (Table S5); photographic depiction of the overall laser setup used in this study (Fig. S01); Venn-diagram of assigned compounds for complex samples (Fig. S02); DBE *vs.* carbon number plots for CHN-, CHO-, CHS- and CHS_2-class of fossil oil samples for all four wavelengths (Fig. S03–S06); DBE distribution of the CH-, CHN-, CHO-, CHS- and CHS_2-class of the fossil oil samples for all four wavelengths, odd and even species are highlighted (Fig. S07–S11); congruence coefficients for the polymer samples measured at all four wavelengths (Fig. S12); comparison of the total ion intensity between the wavelengths for the polymers (Fig. S13). See DOI: https://doi.org/10.1039/d6ay00377j.

Acknowledgements

The authors thank the Interdisciplinary Faculty, Department Life, Light, and Matter at the University of Rostock for providing laboratory space and infrastructure. The authors thank the Deutsche Forschungsgemeinschaft (DFG, German Research Foundation) for funding the Bruker FT-ICR MS (INST 264/56, 142644299) and the European Regional Development Fund (EFRE) for funding the OPO laser system (GHS-18-0008).

References

1 J. B. Fenn, M. Mann, C. K. Meng, S. F. Wong and C. M. Whitehouse, Electrospray ionization for mass spectrometry of large biomolecules, *Science*, 1989, **246**, 64–71.
2 C. Mase, M. Sueur, H. Lavanant, C. P. Rüger, P. Giusti and C. Afonso, Ion Source Complementarity for Characterization of Complex Organic Mixtures Using Fourier Transform Mass Spectrometry: A Review, *Mass Spectrom. Rev.*, 2025, **44**, 808–829.
3 P. Liigand, K. Kaupmees, K. Haav, J. Liigand, I. Leito, M. Girod, R. Antoine and A. Kruve, Think Negative: Finding the Best Electrospray Ionization/MS Mode for Your Analyte, *Anal. Chem.*, 2017, **89**, 5665–5668.
4 T. Kind and O. Fiehn, Advances in structure elucidation of small molecules using mass spectrometry, *Bioanal. Rev.*, 2010, **2**, 23–60.
5 L. Sleno and D. A. Volmer, Ion activation methods for tandem mass spectrometry, *J. Mass Spectrom.*, 2004, **39**, 1091–1112.
6 S. Alanazi, Recent Advances in Liquid Chromatography-Mass Spectrometry (LC-MS) Applications in Biological and Applied Sciences, *Anal. Sci. Adv.*, 2025, **6**, e70024.
7 X. Zhang, K. J. Gillig and W. Sun, Recent advances in ion mobility instrumentation for targeted analysis, *TrAC, Trends Anal. Chem.*, 2026, **194**, 118507.
8 D. G. Delafield, G. Lu, C. J. Kaminsky and L. Li, High-end ion mobility mass spectrometry: a current review of analytical capacity in omics applications and structural investigations, *TrAC, Trends Anal. Chem.*, 2022, **157**, 116761.
9 C. P. Rüger, A. Neumann, M. Sklorz and R. Zimmermann, Atmospheric Pressure Single Photon Laser Ionization (APSPLI) Mass Spectrometry Using a 157 nm Fluorine Excimer Laser for Sensitive and Selective Detection of Non- to Semipolar Hydrocarbons, *Anal. Chem.*, 2021, **93**, 3691–3697.
10 A. Neumann, O. Tiemann, H. J. Hansen, C. P. Rüger and R. Zimmermann, Detailed Comparison of Xenon APPI (9.6/

8.4 eV), Krypton APPI (10.6/10.0 eV), APCI, and APLI (266 nm) for Gas Chromatography High Resolution Mass Spectrometry of Standards and Complex Mixtures, *J. Am. Soc. Mass Spectrom.*, 2023, **34**, 1632–1646.

11 T. Streibel and R. Zimmermann, Resonance-enhanced multiphoton ionization mass spectrometry (REMPI-MS): applications for process analysis, *Annu. Rev. Anal. Chem.*, 2014, **7**, 361–381.

12 C. Schwarz, F. Etscheidt, C. Gehm, J. Passig, S. Ehlert, T. Streibel and R. Zimmermann, Resonance-Enhanced Multiphoton Ionization Spectroscopy of Monocyclic and Polycyclic Aromatic Hydrocarbons in the Gas Phase, *Rapid Commun. Mass Spectrom.*, 2025, **39**, e10096.

13 F. Etscheidt, C. P. Rüger, C. Schwarz, O. Tiemann, A. Neumann, H. J. Hansen, T. Streibel, S. Ehlert and R. Zimmermann, Atmospheric Pressure Laser Ionization Mass Spectrometry with Tunable UV Wavelength Utilizing an Optical Parametric Oscillator, *Anal. Chem.*, 2025, **97**, 676–685.

14 C. P. Rüger, O. Tiemann, A. Neumann, T. Streibel and R. Zimmermann, Review on Evolved Gas Analysis Mass Spectrometry with Soft Photoionization for the Chemical Description of Petroleum, Petroleum-Derived Materials, and Alternative Feedstocks, *Energy Fuels*, 2021, **35**, 18308–18332.

15 C. P. Rüger, J. Le Maître, E. Riches, M. Palmer, J. Orasche, O. Sippula, J. Jokiniemi, C. Afonso, P. Giusti and R. Zimmermann, Cyclic Ion Mobility Spectrometry Coupled to High-Resolution Time-of-Flight Mass Spectrometry Equipped with Atmospheric Solid Analysis Probe for the Molecular Characterization of Combustion Particulate Matter, *J. Am. Soc. Mass Spectrom.*, 2021, **32**, 206–217.

16 O. Lacroix-Andrivet, C. Castilla, C. Rüger, M. Hubert-Roux, A. L. M. Siqueira, P. Giusti and C. Afonso, Direct Insertion Analysis of Polymer-Modified Bitumen by Atmospheric Pressure Chemical Ionization Ultrahigh-Resolution Mass Spectrometry, *Energy Fuels*, 2021, **35**, 2165–2173.

17 C. Castilla, C. P. Rüger, H. Lavanant and C. Afonso, Ion mobility mass spectrometry of in situ generated biomass pyrolysis products, *J. Anal. Appl. Pyrolysis*, 2021, **156**, 105164.

18 C. Castilla, C. P. Rüger, S. Marcotte, H. Lavanant and C. Afonso, Direct Inlet Probe Atmospheric Pressure Photo and Chemical Ionization Coupled to Ultrahigh Resolution Mass Spectrometry for the Description of Lignocellulosic Biomass, *J. Am. Soc. Mass Spectrom.*, 2020, **31**, 822–831.

19 C. Barrère, F. Maire, C. Afonso and P. Giusti, Atmospheric solid analysis probe-ion mobility mass spectrometry of polypropylene, *Anal. Chem.*, 2012, **84**, 9349–9354.

20 E. Cossoul, M. Hubert-Roux, M. Sebban, F. Churlaud, H. Oulyadi and C. Afonso, Evaluation of atmospheric solid analysis probe ionization coupled to ion mobility mass spectrometry for characterization of poly(ether ether ketone) polymers, *Anal. Chim. Acta*, 2015, **856**, 46–53.

21 M. Farenc, M. Witt, K. Craven, C. Barrère-Mangote, C. Afonso and P. Giusti, Characterization of Polyolefin Pyrolysis Species Produced Under Ambient Conditions by Fourier Transform Ion Cyclotron Resonance Mass Spectrometry and Ion Mobility-Mass Spectrometry, *J. Am. Soc. Mass Spectrom.*, 2017, **28**, 507–514.

22 U. Käfer, T. Gröger, C. J. Rohbogner, D. Struckmeier, M. R. Saraji-Bozorgzad, T. Wilharm and R. Zimmermann, Detailed Chemical Characterization of Bunker Fuels by High-Resolution Time-of-Flight Mass Spectrometry Hyphenated to GC × GC and Thermal Analysis, *Energy Fuels*, 2019, **33**, 10745–10755.

23 U. Käfer, T. Gröger, C. P. Rüger, H. Czech, M. Saraji-Bozorgzad, T. Wilharm and R. Zimmermann, Direct inlet probe - high-resolution time-of-flight mass spectrometry as fast technique for the chemical description of complex high-boiling samples, *Talanta*, 2019, **202**, 308–316.

24 A. L. M. Siqueira, M. Beaumesnil, M. Hubert-Roux, C. Loutelier-Bourhis, C. Afonso, S. Pondaven, Y. Bai and A. Racaud, Characterization of polyalphaolefins using halogen anion attachment in atmospheric pressure photoionization coupled with ion mobility spectrometry-mass spectrometry, *Analyst*, 2018, **143**, 3934–3940.

25 E. Rytkönen, J. Rouvinen, J. Jänis and M. Mäkinen, Atmospheric Pressure Photoionization with Halogen Anion Attachment for Mass Spectrometric Analysis of Hydrocarbons and Hydrocarbon-Based Polymers, *J. Am. Soc. Mass Spectrom.*, 2024, **35**, 3147–3156.

26 R. Gholami, A. Alvarez-Majmutov and J. Chen, Process modelling and simulation of bitumen partial upgrading: analysis of solvent deasphalting-thermal cracking configuration, *Can. J. Chem. Eng.*, 2022, **100**, 1516–1529.

27 M. L. Chacón-Patiño, A. Neumann, C. P. Rüger, P. G. Bomben, L. Friederici, R. Zimmermann, E. Frank, P. Kreis, M. R. Buchmeiser and M. R. Gray, Chemistry and Properties of Carbon Fiber Feedstocks from Bitumen Asphaltenes, *Energy Fuels*, 2023, **37**, 5341–5360.

28 Center for Marine Debris Research, *Polymer Kit 1.0 to Harmonize Plastic Pollution Research*, accessed 2 March 2026, https://www.hpu.edu/cncs/cmdr/img/polymerkit1.0_marketingbrochure.pdf.

29 C. P. Rüger, T. Schwemer, M. Sklorz, P. B. O'Connor, M. P. Barrow and R. Zimmermann, Comprehensive chemical comparison of fuel composition and aerosol particles emitted from a ship diesel engine by gas chromatography atmospheric pressure chemical ionisation ultra-high resolution mass spectrometry with improved data processing routines, *Eur. J. Mass Spectrom.*, 2017, **23**, 28–39.

30 K. Grönlund, V. H. Nissinen, I. Rytöluoto, M. Mosallaei, J. Mikkonen, K. Korpijärvi, P. Auvinen, M. Suvanto, J. J. Saarinen and J. Jänis, Direct Mass Spectrometric Analysis of Brominated Flame Retardants in Synthetic Polymers, *ACS Omega*, 2024, **9**, 33011–33021.

31 V. Sierra-Jimenez, T. Voellinger, V. Carré, F. Chejne, S. Schramm, F. Aubriet and M. Garcia-Perez, Exploring Cellulose Fast Pyrolysis Secondary Reactions Through Reactive Molecular Dynamics and Direct Insertion Probe Fourier Transform Ion Cyclotron Resonance Mass Spectrometry, *Energy Fuels*, 2025, **39**, 9860–9873.

32 T. J. Kauppila, H. Kersten and T. Benter, The ionization mechanisms in direct and dopant-assisted atmospheric pressure photoionization and atmospheric pressure laser ionization, *J. Am. Soc. Mass Spectrom.*, 2014, **25**, 1870–1881.
33 T. J. Kauppila, J. A. Syage and T. Benter, Recent developments in atmospheric pressure photoionization-mass spectrometry, *Mass Spectrom. Rev.*, 2017, **36**, 423–449.
34 R. Shinoda, K. Takahashi, S. Ichikawa, M. Wakayama, A. Kobayashi, S. Miyagawa and T. Uchimura, Using SPME-GC/REMPI-TOFMS to Measure the Volatile Odor-Active Compounds in Freshly Cooked Rice, *ACS Omega*, 2020, **5**, 20638–20642.
35 I. J. Amster, Fourier Transform Mass Spectrometry, *J. Mass Spectrom.*, 1996, **31**, 1325–1337.
36 C. Gehm, T. Streibel, J. Passig and R. Zimmermann, Determination of Relative Ionization Cross Sections for Resonance Enhanced Multiphoton Ionization of Polycyclic Aromatic Hydrocarbons, *Appl. Sci.*, 2018, **8**, 1617.
37 A. Samanta, C. Devadoss and R. W. Fessenden, Picosecond time-resolved absorption and emission studies of the singlet excited states of acenaphthylene, *J. Phys. Chem.*, 1990, **94**, 7106–7110.
38 H. Brockmann and W. Müller, Hydroxy-tetracenchinone, *Chem. Ber.*, 1959, **92**, 1164–1170.
39 R. Tembreull, C. H. Sin, P. Li, H. M. Pang and D. M. Lubman, Applicability of resonant two-photon ionization in supersonic beam mass spectrometry to halogenated aromatic hydrocarbons, *Anal. Chem.*, 1985, **57**, 1186–1192.
40 C. F. Dion and E. R. Bernstein, On the low-lying Rydberg states of azabenzenes, *J. Chem. Phys.*, 1995, **103**, 4907–4913.
41 M. Tsubouchi and T. Suzuki, Femtosecond Photoelectron Imaging on Pyridine: Ultrafast Electronic Dephasing from the S1 (n π^*) State and Rydberg State Energetics, *J. Phys. Chem. A*, 2003, **107**, 10897–10903.
42 J. M. Purcell, R. P. Rodgers, C. L. Hendrickson and A. G. Marshall, Speciation of nitrogen containing aromatics by atmospheric pressure photoionization or electrospray ionization fourier transform ion cyclotron resonance mass spectrometry, *J. Am. Soc. Mass Spectrom.*, 2007, **18**, 1265–1273.
43 A. Marshall, A. Clark, K. W. D. Ledingham, J. Sander, R. P. Singhal, C. Kosmidis and R. M. Deas, Detection and identification of explosives compounds using laser ionization time-of-flight techniques, *Rapid Commun. Mass Spectrom.*, 1994, **8**, 521–526.
44 J. M. Headrick, T. A. Reichardt, T. B. Settersten, R. P. Bambha and D. A. V. Kliner, Application of laser photofragmentation-resonance enhanced multiphoton ionization to ion mobility spectrometry, *Appl. Opt.*, 2010, **49**, 2204–2214.
45 S. D. Roberson and R. C. Sausa, Laser-based detection of TNT and RDX residues in real time under ambient conditions, *Appl. Spectrosc.*, 2010, **64**, 760–766.
46 R. Weinkauf, P. Aicher, G. Wesley, J. Grotemeyer and E. W. Schlag, Femtosecond versus Nanosecond Multiphoton Ionization and Dissociation of Large Molecules, *J. Phys. Chem.*, 1994, **98**, 8381–8391.
47 Y. Watanabe-Ezoe, X. Li, T. Imasaka, T. Uchimura and T. Imasaka, Gas chromatography/femtosecond multiphoton ionization/time-of-flight mass spectrometry of dioxins, *Anal. Chem.*, 2010, **82**, 6519–6525.
48 T. Fujii, T. Imasaka and T. Imasaka, Use of chemical conversion for determination of nitrated aromatic hydrocarbons using femtosecond ionization mass spectrometry, *Anal. Chim. Acta*, 2017, **996**, 48–53.
49 H. B. Klevens and J. R. Platt, Spectral Resemblances of Cata-Condensed Hydrocarbons, *J. Chem. Phys.*, 1949, **17**, 470–481.
50 G. D'Arcangelo, T. Reichenauer, J. Bloino and S. Schlücker, Insights into the Lowest Excited State of Anthracene: Kerr-Gated UV Resonance Raman Spectroscopy (S1 ← S0) with Tunable Excitation and DFT Analysis, *J. Phys. Chem. Lett.*, 2025, 10180–10186.
51 H. Kersten, V. Funcke, M. Lorenz, K. J. Brockmann, T. Benter and R. O'Brien, Evidence of neutral radical induced analyte ion transformations in APPI and near-VUV APLI, *J. Am. Soc. Mass Spectrom.*, 2009, **20**, 1868–1880.
52 W. Schrader, S. K. Panda, K. J. Brockmann and T. Benter, Characterization of non-polar aromatic hydrocarbons in crude oil using atmospheric pressure laser ionization and Fourier transform ion cyclotron resonance mass spectrometry (APLI FT-ICR MS), *Analyst*, 2008, **133**, 867–869.
53 M. L. Chacón-Patiño, M. R. Gray, C. Rüger, D. F. Smith, T. J. Glattke, S. F. Niles, A. Neumann, C. R. Weisbrod, A. Yen, A. M. McKenna, P. Giusti, B. Bouyssiere, C. Barrère-Mangote, H. Yarranton, C. L. Hendrickson, A. G. Marshall and R. P. Rodgers, Lessons Learned from a Decade-Long Assessment of Asphaltenes by Ultrahigh-Resolution Mass Spectrometry and Implications for Complex Mixture Analysis, *Energy Fuels*, 2021, **35**, 16335–16376.
54 A. Gaspar, E. Zellermann, S. Lababidi, J. Reece and W. Schrader, Characterization of Saturates, Aromatics, Resins, and Asphaltenes Heavy Crude Oil Fractions by Atmospheric Pressure Laser Ionization Fourier Transform Ion Cyclotron Resonance Mass Spectrometry, *Energy Fuels*, 2012, **26**, 3481–3487.
55 C. Kruth, H. Czech, M. Sklorz, J. Passig, S. Ehlert, A. Cappiello and R. Zimmermann, Direct Infusion Resonance-Enhanced Multiphoton Ionization Mass Spectrometry of Liquid Samples under Vacuum Conditions, *Anal. Chem.*, 2017, **89**, 10917–10923.
56 J. B. Thiäner and C. Achten, Liquid chromatography-atmospheric pressure laser ionization-mass spectrometry (LC-APLI-MS) analysis of polycyclic aromatic hydrocarbons with 6-8 rings in the environment, *J. Phys. Chem. Lett.*, 2017, **409**, 1737–1747.
57 L. Renzi and W. Peirong, PAH in fossil fuels and their geochemical significance, *J. Southeast Asian Earth Sci.*, 1991, **5**, 257–262.
58 N. Kateris, A. S. Jayaraman and H. Wang, HOMO-LUMO gaps of large polycyclic aromatic hydrocarbons and their implication on the quantum confinement behavior of flame-formed carbon nanoparticles, *Proc. Combust. Inst.*, 2023, **39**, 1069–1077.

59 M. Krykunov, S. Grimme and T. Ziegler, Accurate Theoretical Description of the (1)La and (1)Lb Excited States in Acenes Using the All Order Constricted Variational Density Functional Theory Method and the Local Density Approximation, *J. Chem. Theor. Comput.*, 2012, **8**, 4434–4440.
60 M. L. Chacón-Patiño, S. M. Rowland and R. P. Rodgers, in *The Boduszynski Continuum: Contributions to the Understanding of the Molecular Composition of Petroleum*, ed. C. Ovalles and M. E. Moir, American Chemical Society, Washington, DC, 2018, pp. 113–171.
61 C. S. Hsu, K. Qian and W. K. Robbins, Nitrogen speciation of polar petroleum compounds by compound class separation and on-line liquid chromatography – mass spectrometry (LC-MS), *J. High Resolut. Chromatogr.*, 1994, **17**, 271–276.
62 J. Paudel, D. Carter, P. d. B. Harrington and B. J. Bythell, Fragmentation Chemistry of Tetrahydrocarbazole Analogs Relevant to Nitrogen Compounds in Heavy Crude Oils, *Energy Fuels*, 2025, **39**, 23259–23271.
63 J. Le Maître, B. Paupy, M. Hubert-Roux, S. Marceau, C. Rüger, C. Afonso and P. Giusti, Structural Analysis of Neutral Nitrogen Compounds Refractory to the Hydrodenitrogenation Process of Heavy Oil Fractions by High-Resolution Tandem Mass Spectrometry and Ion Mobility–Mass Spectrometry, *Energy Fuels*, 2020, **34**, 9328–9338.
64 L. Schwalb, O. Tiemann, U. Käfer, T. Gröger, C. P. Rüger, G. Gayko and R. Zimmermann, Analysis of complex drugs by comprehensive two-dimensional gas chromatography and high-resolution mass spectrometry: detailed chemical description of the active pharmaceutical ingredient sodium bituminosulfonate and its process intermediates, *J. Phys. Chem. Lett.*, 2023, **415**, 2471–2481.
65 O. Tiemann, C. P. Rüger, L. Schwalb, M. L. Chacón-Patiño, T. Gröger and R. Zimmermann, Rock-to-Pharma: Characterization of Shale Oil-Based Nonbiological Complex Drugs along the Production Process by High-Resolution Mass Spectrometry, *Anal. Chem.*, 2024, **96**, 13050–13060.
66 U. Boesl, H. J. Neusser and E. W. Schlag, Multi-photon ionization in the mass spectrometry of polyatomic molecules: cross sections, *Chem. Phys.*, 1981, **55**, 193–204.
67 Y. Zhou, S. Feng, H. Li, L. Zhao, Z. Pan, Z. Wu, C. Shi, Z. Zhen, Z. Zhou, H. Zhang and J. Yan, Initial products analysis and mechanistic insights into polystyrene pyrolysis via in-situ photoionization mass spectrometry, *Chem. Eng. J.*, 2025, **511**, 162118.
68 R. N. Datta, N. M. Huntink, S. Datta and A. G. Talma, Rubber Vulcanizates Degradation and Stabilization, *Rubber Chem. Technol.*, 2007, **80**, 436–480.
69 R. H. Krüger, C. Boissiére, K. Klein-Hartwig and H.-J. Kretzschmar, New phenylenediamine antiozonants for commodities based on natural and synthetic rubber, *Food Addit. Contam.*, 2005, **22**, 968–974.
70 F. Chen and J. Qian, Studies of the thermal degradation of waste rubber, *Waste Manag.*, 2003, **23**, 463–467.

